Synthesis of a robust linear structural feedback linearization scheme for an experimental quadrotor

Luis Angel A Blas, Moisés E. Bonilla, Sergio Salazar, Michel Malabre, Vadim Azhmyakov

Synthesis of a robust linear structural feedback linearization scheme for an experimental quadrotor

L.A. Blas[1], M. Bonilla[1], S. Salazar[2], M. Malabre[3] and V. Azhmyakov[4]

***Abstract*— In this paper, we show in detail a synthesis procedure of the control scheme recently proposed in [3]. This control scheme has the advantage of combining the classical linear control techniques with the sophisticated robust control techniques. This control scheme is specially *ad hoc* for unmanned aircraft vehicles, where it is important not only to reject the actual nonlinearities and the unexpected changes of the structure, but also to look for the simplicity and effectiveness of the control scheme.**

I. INTRODUCTION

Recently, there has been a great interest in finding simple and effective control schemes for unmanned aircraft vehicles, able to reject the actual nonlinearities and the unexpected changes of structure. In [6], the authors present two types of nonlinear controllers for an autonomous quadrotor helicopter. However, to program this control scheme in the embedded autopilot of the quadrotor is rather difficult due to the needed derivative estimations. In [13], the authors present attitude and trajectory tracking control designs based on an inner/outer-loop control structure for normal flight conditions. Once again, to program this control scheme in the embedded autopilot of the quadrotor is rather difficult due to the needed derivative estimations. In [7], the authors propose a robust controller based on the time-scale separation approach to achieve the automatic take-off, hovering, trajectory tracking, and landing missions for a quadrotor helicopter. The authors only show experimental results in indoor environments.

In this paper, we present a synthesis procedure of the recently robust linear control scheme proposed in [3], which is based on failure detection techniques. Such a linear control approach is intended to reject linearly structured uncertainties, which are treated as failure signals affecting the systems dynamics. The implementability and efficiency of the proposed robust control methodology is illustrated with a quadrotor laboratory prototype in hover flying. We present simulation results and experimental results in open field (outdoor environments).

*The Ph.D. Student Luis Angel Blas Sanchez is sponsored by CONACyT México.

[1]L.A. Blas and M. Bonilla are with CINVESTAV-IPN, Control Automático, UMI 3175 CINVESTAV-CNRS. A.P. 14-740. México 07000. anghel_lam@hotmail.com, mbonilla@cinvestav.mx

[2]S. Salazar is with CINVESTAV-IPN, Sistemas Autónomos de Navegación Aérea Y Submarina, UMI 3175 CINVESTAV-CNRS. A.P. 14-740. México 07000. sergio.salazar.cruz@gmail.com

[3]M. Malabre is with CNRS, LS2N, UMR 6004, Nantes, France. Michel.Malabre@ls2n.fr

[4]V. Azhmyakov is with Department of Mathematical Sciences, Universidad EAFIT, Medellin, Republic of Colombia. vazhmyako@eafit.edu.co

In Section II, we describe the quadrotor laboratory prototype. In Section III, we give the necessary preliminaries to synthesize the control scheme recently proposed in [3]. In Section IV, we synthesize the *exact structural feedback linearization* and the *robust asymptotic feedback linearization* for the dynamics of the longitudinal trajectory x together with the rotational pitch trajectory θ of the quadrotor. In Section V, we do some simulation for tuning our control scheme. In Section VI, we test our proposition in open field. In Section VII, we conclude.

II. QUADROTOR DESCRIPTION

Let us consider a quadrotor where the total mass is M_q, the moments of inertia about axis ox, oy and oz are:[1] $\mathcal{I}_{xx}$, $\mathcal{I}_{yy}$ and $\mathcal{I}_{zz}$, and the distance of each rotor with respect to the centre of gravity of the quadrotor is L_m (see Fig. 4). The motion is referred to a fixed orthogonal axis set (earth axes) ($o\mathsf{xyz}$), where $o\mathsf{z}$ points vertically down along the gravity vector $\begin{bmatrix} 0 & 0 & g \end{bmatrix}^T$, and the origin o is located at the desired height $\bar{\mathsf{z}}$, above the ground level. ϕ, θ and ψ are the Euler angles, roll, pitch and yaw, measured respectively over the axis $o_B\mathsf{x}_B$, $o_B\mathsf{y}_B$ and $o_B\mathsf{z}_B$; where $(o_B\mathsf{x}_B\mathsf{y}_B\mathsf{z}_B)$ is the body axis system, with its origin o_B fixed at the centre of gravity of the quadrotor. We denote: $\eta = \begin{bmatrix} \phi & \theta & \psi \end{bmatrix}^T$. The quadrotor is represented by the following state space representations (see [2] for details):

a) State representation of the $\mathsf{x}-\theta$ dynamics:

$$\frac{\mathrm{d}}{\mathrm{d}t}x_{\mathsf{x}} = \mathrm{A}_{\mathsf{x}}x_{\mathsf{x}} + B_{\mathsf{x}}u_{\mathsf{x}} + S_{\mathsf{x}}q_{o\mathsf{x}}\,, \quad \mathsf{x} = C_{\mathsf{x}}x_{\mathsf{x}}\,, \tag{2.1}$$

where $x_{\mathsf{x}} = \begin{bmatrix}\mathsf{x} & \mathrm{d}\mathsf{x}/\mathrm{d}t & \theta & \mathrm{d}\theta/\mathrm{d}t\end{bmatrix}^T$, $q_{o\mathsf{x}} = \begin{bmatrix}q_{\mathsf{x}} & q_\theta\end{bmatrix}^T$, and the matrices A_{x}, B_{x}, S_{x} and C_{x}^T are, respectively,

$$\begin{bmatrix}0&1&0&0\\0&0&-g&0\\0&0&0&1\\0&0&0&0\end{bmatrix}, \begin{bmatrix}0\\0\\0\\1/\mathcal{I}_{yy}\end{bmatrix}, \begin{bmatrix}0&0\\1&0\\0&0\\0&1\end{bmatrix} \text{ and } \begin{bmatrix}1\\0\\0\\0\end{bmatrix} \tag{2.2}$$

b) State representation of the $\mathsf{y}-\phi$ dynamics:

$$\frac{\mathrm{d}}{\mathrm{d}t}x_{\mathsf{y}} = \mathrm{A}_{\mathsf{y}}x_{\mathsf{y}} + B_{\mathsf{y}}u_{\mathsf{y}} + S_{\mathsf{y}}q_{o\mathsf{y}}\,, \quad \mathsf{y} = C_{\mathsf{y}}x_{\mathsf{y}}\,, \tag{2.3}$$

where $x_{\mathsf{y}} = \begin{bmatrix}\mathsf{y} & \mathrm{d}\mathsf{y}/\mathrm{d}t & \phi & \mathrm{d}\phi/\mathrm{d}t\end{bmatrix}^T$, $q_{o\mathsf{y}} = \begin{bmatrix}q_{\mathsf{y}} & q_\phi\end{bmatrix}^T$, and the matrices A_{y}, B_{y}, S_{y} and C_{y}^T are, respectively,

$$\begin{bmatrix}0&1&0&0\\0&0&g&0\\0&0&0&1\\0&0&0&0\end{bmatrix}, \begin{bmatrix}0\\0\\0\\1/\mathcal{I}_{xx}\end{bmatrix}, \begin{bmatrix}0&0\\1&0\\0&0\\0&1\end{bmatrix} \text{ and } \begin{bmatrix}1\\0\\0\\0\end{bmatrix} \tag{2.4}$$

[1]Since the quadrotor is mechanically symmetric its cross inertia are zero.

c) State representation of the ψ dynamics:

$$\frac{\mathrm{d}}{\mathrm{d}t}x_\psi = \mathrm{A}_\psi x_\psi + B_\psi u_\psi + S_\psi q_\psi\,, \quad \psi = C_\psi x_\psi\,,$$

where $x_\psi = \begin{bmatrix}\psi & \mathrm{d}\psi/\mathrm{d}t\end{bmatrix}^T$, and the matrices A_ψ, B_ψ, S_ψ and C_ψ^T are, respectively, $\begin{bmatrix}0 & 1\\ 0 & 0\end{bmatrix}$, $\begin{bmatrix}0\\ 1/\mathcal{I}_{zz}\end{bmatrix}$, $\begin{bmatrix}0\\ 1\end{bmatrix}$ and $\begin{bmatrix}1\\ 0\end{bmatrix}$.

d) State representation of the z dynamics:

$$\frac{\mathrm{d}}{\mathrm{d}t}x_\mathsf{z} = \mathrm{A}_\mathsf{z} x_\mathsf{z} + B_\mathsf{z}\Delta u_\mathsf{z} + S_\mathsf{z} q_\mathsf{z}\,, \quad \mathsf{z} = C_\mathsf{z} x_\mathsf{z}\,, \tag{2.5}$$

where $x_\mathsf{z} = \begin{bmatrix}\mathsf{z} & \mathrm{d}\mathsf{z}/\mathrm{d}t\end{bmatrix}^T$, and the matrices A_z, B_z, S_z and C_z^T are, respectively, $\begin{bmatrix}0 & 1\\ 0 & 0\end{bmatrix}$, $\begin{bmatrix}0\\ 1/M_q\end{bmatrix}$, $\begin{bmatrix}0\\ 1\end{bmatrix}$ and $\begin{bmatrix}1\\ 0\end{bmatrix}$

In the fifth Section of [2], we show how the incremental control actions, u_x, u_y, $u_\mathsf{z} = \Delta u_\mathsf{z} - M_q g$ and u_ψ, are related with the thrusters of the four rotors, $\mathfrak{f}_1$, $\mathfrak{f}_2$, $\mathfrak{f}_3$ and $\mathfrak{f}_4$. The nonlinear signals, q_x, q_y, q_z, q_ϕ, q_θ and q_ψ, are:

$$\begin{bmatrix}q_\mathsf{x}\\ q_\mathsf{y}\\ q_\mathsf{z}\end{bmatrix} = \begin{bmatrix}\theta - q_{\mathsf{xx}}\\ -\phi - q_{\mathsf{yy}}\\ -q_{\mathsf{zz}}\end{bmatrix} g + \frac{1}{M_q}\begin{bmatrix}q_{\mathsf{xx}}\\ q_{\mathsf{yy}}\\ q_{\mathsf{zz}}\end{bmatrix}\Delta u_\mathsf{z}\,, \tag{2.6}$$

$$\begin{bmatrix}q_\phi\\ q_\theta\\ q_\psi\end{bmatrix} = \left(\mathbb{J}^{-1}(\eta) - \mathbb{J}^{-1}(0)\right)\tau - \mathbb{J}^{-1}(\eta)C(\eta, \mathrm{d}\eta/\mathrm{d}t)\frac{\mathrm{d}\eta}{\mathrm{d}t}\,, \tag{2.7}$$

where $\mathbb{J}$ and $C(\eta, \mathrm{d}\eta/\mathrm{d}t)$ are the inertial and the Coriolis matrices, defined in the Appendix of [2], and:[2]

$$\begin{gathered}q_{\mathsf{xx}} = c_\phi s_\theta c_\phi + s_\phi s_\psi\,, \quad q_{\mathsf{yy}} = c_\phi s_\theta s_\psi - s_\phi c_\psi\,,\\ q_{\mathsf{zz}} = c_\phi c_\theta - 1\,.\end{gathered} \tag{2.8}$$

III. PRELIMINAIRES

Let us consider a nonlinear system described by the following nonlinear state space representation:

$$\frac{\mathrm{d}}{\mathrm{d}t}x(t) = Ax(t) + Bu(t) + Sq(x(t), u(t)), \quad y(t) = Cx(t), \tag{3.1}$$

where $u \in \mathbb{R}^m$ and $y \in \mathbb{R}^p$ are the input and the output, respectively, $x \in \mathbb{R}^n$ is the state and $q \in \mathbb{R}^\mu$ is a nonlinear perturbation signal, here called an uncertainty vector. We do the following assumption:

H1: Structural hypothesis:

1) $\ker B = 0$.
2) The pair (A, B) is controllable, namely (see for example [12]): $\mathbb{R}^n = \langle A \,|\, \operatorname{Im} B\rangle = \operatorname{Im} B + A \operatorname{Im} B + \cdots + A^{n-1}\operatorname{Im} B$.
3) The pair (C, A) is observable.

We need two results stated in [3].

Lemma 1 ([3]): Under assumptions **H1.1** and **H1.2**, there exist two linear transformations, $M : \mathbb{R}^n \to \mathbb{R}^n$ and $X : \mathbb{R}^n \to \mathbb{R}^m$, solving the matrix equality:

$$AM + BX = \mathrm{I}\,, \tag{3.2}$$

satisfying: $X = B^\ell(\mathrm{I} - AM)$ and $M^n = 0$, where $B^\ell : \mathbb{R}^n \to \mathbb{R}^m$ is a left inverse of $B : \mathbb{R}^m \to \mathbb{R}^n$, $B^\ell B = \mathrm{I}$, and $M : \mathbb{R}^n \to \mathbb{R}^n$ has a nilpotent index not greater than n.

Equality (3.2) directly follows from **H1.2**: $\mathbb{R}^n = \langle A \,|\, \operatorname{Im} B\rangle \subset \operatorname{Im} B + \operatorname{Im} A \subset \mathbb{R}^n$; for the other ones see the proof in [3].

Defining:

$$\mathcal{C}_{(M,\,S)} = \begin{bmatrix} S & MS & \cdots & M^{(n-1)}S \end{bmatrix}, \tag{3.3}$$

$$\Psi_n(\mathrm{d}/\mathrm{d}t) = \begin{bmatrix} \mathrm{I} & \mathrm{I}\,\mathrm{d}/\mathrm{d}t & \cdots & \mathrm{I}\,\mathrm{d}^{n-1}/\mathrm{d}t^{n-1} \end{bmatrix}^T, \tag{3.4}$$

and assuming:

H2: The subspace $M \operatorname{Im} S$ is contained in the unobservable subspace $\langle \ker C \,|\, M\rangle = \ker C \cap M^{-1} \ker C \cap \cdots \cap M^{-(n-1)} \ker C$, namely:

$$CM\mathcal{C}_{(M,\,S)} = 0, \tag{3.5}$$

the following Theorem is obtained:

Theorem 1 ([3]): Given the linear transformations M and X from Lemma 1, consider the following change of variable:

$$\zeta(t) = x(t) + M\mathcal{C}_{(M,\,S)}\,\Psi_n(\mathrm{d}/\mathrm{d}t)\,q(x(t),\,u(t))\,. \tag{3.6}$$

Under Assumptions **H1.1**, **H1.2** and **H2**, the state representation (3.1) is externally equivalent to the following[3]:

$$\frac{\mathrm{d}}{\mathrm{d}t}\zeta(t) = A\zeta(t) + B\left(u(t) + q_*(x(t),\,u(t))\right), \quad y(t) = C\zeta(t), \tag{3.7}$$

where the *nonlinear uncertainty signal*, q_*, is given by:

$$q_*(x(t),\,u(t)) = X\mathcal{C}_{(M,\,S)}\,\Psi_n(\mathrm{d}/\mathrm{d}t)\,q(x(t),\,u(t)). \tag{3.8}$$

Theorem 1 is important because it provides us the change of basis (3.6), which aim is to map the uncertainty vector (nonlinear perturbation signal), q, to the nonlinear uncertainty signal (3.8), q_*, contained in $\operatorname{Im} B$. Thus,

$$u(t) = -q_*(x(t),\,u(t)), \tag{3.9}$$

exactly linearizes (3.7).

In the case when it is not possible to reconstruct analytically the *nonlinear uncertainty signal* q_*, or it is a heavy and tedious task to do it, one can still estimate it. For this, we need to add the following assumption:

H3: The state space description $\Sigma(A, B, C)$ (3.1) has no finite invariant zeros at the origin, namely:

$$\operatorname{Im} B \cap A \ker C = 0\,. \tag{3.10}$$

Assumptions **H1.3** and **H3** make it possible to apply results of [1] and to design a robust disturbance rejection (based on the Beard-Jones filter, see [8] and the reference there included):

$$\begin{aligned}&\tfrac{\mathrm{d}}{\mathrm{d}t}w(t) = A_K w(t) - Ky(t) + Bu(t),\\ &\hat{q}_*(t) = -G^\ell(Cw(t) - y(t)), \quad u(t) = -\hat{q}_*(t).\end{aligned} \tag{3.11}$$

[2]We use the abbreviated notations: $(c_\phi,\, c_\theta,\, c_\psi)$ for $(\cos\phi,\, \cos\theta,\, \cos\psi)$ and $(s_\phi,\, s_\theta,\, s_\psi)$ for $(\sin\phi,\, \sin\theta,\, \sin\psi)$.

[3]Recall that two representations are called externally equivalent if the corresponding sets of all possible trajectories for the external variables expressed in an *input/output partition* (u, y) are the same [10], [11].

where $A_K \doteq (A + KC)$ with $K : \mathbb{R}^p \to \mathbb{R}^m$ an output injection such that: $\sigma\{(A + KC)\} \subset \mathbb{C}^-$, and G^ℓ is a left inverse of the static gain $-C(A+KC)^{-1}B$. The remainder generator is expressed as:

$$\frac{\mathrm{d}}{\mathrm{d}t}e(t) = A_K e(t) - Bq_*(x,u),\ \ \hat{q}_*(t) = -G^\ell Ce(t), \quad (3.12)$$

where $e(t) = w(t) - \zeta(t)$. In the case when the classic Laplace transform of $q_*(x,u)$ is well-defined, we have the following transfer function:

$$\mathsf{F}_e(\mathrm{s}) = G^\ell\, C\,(\mathrm{s}\mathrm{I} - A_K)^{-1}\, B\,. \quad (3.13)$$

Under the natural boundedness assumption for $q_*(x,u)$ with a bandwidth ω_q, we have to synthesize a Hurwitz low-pass filter $\mathsf{F}_e(\mathrm{s})$ with a corner frequency ω_c, which aim is to reconstruct $q_*(x,u)$. Indeed, the *nonlinear uncertainty signal* q_* is affecting the closed loop behavior throw the high-pass filter $1 - \mathsf{F}_e(\mathrm{s})$, so the corner frequency ω_c of the low-pass filter $\mathsf{F}_e(\mathrm{s})$ should be sufficiently greater than the bandwidth ω_q, in order to reject q_*. This is with the aim to achieve a robust disturbance in a neighborhood around the equilibrium point $(x,\, u) = (0,\, 0)$, namely:

$$\|q_*(\omega) - \hat{q}_*(\omega)\| \le \|\,(\mathrm{I} - \mathsf{F}_e(\jmath\omega))\, X\mathcal{C}_{(M,\,S)}\Psi_n(\jmath\omega)\|\|q(\omega)\|\,.$$

IV. LINEAR ROBUST CONTROL SYNTHESIS

In this Section, we synthesize the *exact structural feedback linearization* (3.8) and (3.9), and the *robust asymptotic feedback linearization* (3.11), for the $\mathsf{x} - \theta$ dynamics (2.1) and (2.2); the other ones are done in a very similar way.

A. Locally Stabilizing Feedback

Applying the feedback

$$\begin{array}{rcl} u_{\mathsf{x}} & = & F_{\mathsf{x}} x_{\mathsf{x}} + \bar{u}_{\mathsf{x}}\,, \\ F_{\mathsf{x}} & = & \begin{bmatrix} a_{\mathsf{x},4}\mathcal{I}_{yy}/g & a_{\mathsf{x},3}\mathcal{I}_{yy}/g & -a_{\mathsf{x},2}\mathcal{I}_{yy} & -a_{\mathsf{x},1}\mathcal{I}_{yy} \end{bmatrix}, \end{array} \quad (4.1)$$

to (2.1), one gets:

$$\frac{\mathrm{d}}{\mathrm{d}t}x_{\mathsf{x}} = A_{F_{\mathsf{x}}} x_{\mathsf{x}} + B_{\mathsf{x}}\bar{u}_{\mathsf{x}} + S_{\mathsf{x}} q_{o\mathsf{x}}\,, \quad \mathsf{x} = C_{\mathsf{x}} x_{\mathsf{x}}\,, \quad (4.2)$$

where:

$$A_{F_{\mathsf{x}}} = \mathrm{A}_{\mathsf{x}} + B_{\mathsf{x}} F_{\mathsf{x}} = \begin{bmatrix} 0 & 1 & 0 & 0 \\ 0 & 0 & -g & 0 \\ 0 & 0 & 0 & 1 \\ a_{\mathsf{x},4}/g & a_{\mathsf{x},3}/g & -a_{\mathsf{x},2} & -a_{\mathsf{x},1} \end{bmatrix}, \quad (4.3)$$

with the following Hurwitz characteristic polynomial:

$$\pi_{x_{\mathsf{x}}}(\mathrm{s}) = \det(\mathrm{s}\mathrm{I} - A_{F_{\mathsf{x}}}) = \mathrm{s}^4 + a_{\mathsf{x},1}\mathrm{s}^3 + a_{\mathsf{x},2}\mathrm{s}^2 + a_{\mathsf{x},3}\mathrm{s} + a_{\mathsf{x},4}\,. \quad (4.4)$$

B. Exact Structural Feedback Linearization

The matrices M_{x} and X_{x} solving the algebraic equation (*cf.* (3.2)): $A_{F_{\mathsf{x}}} M_{\mathsf{x}} + B_{\mathsf{x}} X_{\mathsf{x}} = \mathrm{I}_4$, and the operators (3.3) and (3.4) are:

$$\begin{array}{l} M_{\mathsf{x}} = \begin{bmatrix} 0 & 0 & 0 & 0 \\ 1 & 0 & 0 & 0 \\ 0 & -1/g & 0 & 0 \\ 0 & 0 & 1 & 0 \end{bmatrix}, \\ X_{\mathsf{x}} = \begin{bmatrix} -a_{\mathsf{x},3}\mathcal{I}_{yy}/g & -a_{\mathsf{x},2}\mathcal{I}_{yy}/g & a_{\mathsf{x},1}\mathcal{I}_{yy} & \mathcal{I}_{yy} \end{bmatrix}, \\ \mathcal{C}_{(M_{\mathsf{x}},\,S_{\mathsf{x}})} = \begin{bmatrix} 0 & 0 & 0 & 0 & 0 & 0 & 0 & 0 \\ 1 & 0 & 0 & 0 & 0 & 0 & 0 & 0 \\ 0 & 0 & -1/g & 0 & 0 & 0 & 0 & 0 \\ 0 & 1 & 0 & 0 & -1/g & 0 & 0 & 0 \end{bmatrix}, \\ \Psi_4(\mathrm{d}/\mathrm{d}t) = \begin{bmatrix} \mathrm{I}_2 & \mathrm{I}_2\,\mathrm{d}/\mathrm{d}t & \mathrm{I}_2\,\mathrm{d}^2/\mathrm{d}t^2 & \mathrm{I}_2\,\mathrm{d}^3/\mathrm{d}t^3 \end{bmatrix}^T. \end{array} \quad (4.5)$$

Note that: $M_{\mathsf{x}}^4 = 0$ and $C_{\mathsf{x}} M_{\mathsf{x}} \mathcal{C}_{(M_{\mathsf{x}},\,S_{\mathsf{x}})} = 0$. The change of variable (3.6) is (*cf.* (4.5)):

$$\zeta_{\mathsf{x}} = x_{\mathsf{x}} - \left(\frac{1}{g}\right) \begin{bmatrix} 0 & 0 \\ 0 & 0 \\ 1 & 0 \\ \mathrm{d}/\mathrm{d}t & 0 \end{bmatrix} \begin{bmatrix} q_{\mathsf{x}} \\ q_\theta \end{bmatrix}. \quad (4.6)$$

The nonlinear uncertainty signal (3.8) is (*cf.* (4.5)):

$$q_{\mathsf{x},*} = -\frac{\mathcal{I}_{yy}}{g}\left(a_{\mathsf{x},2} + a_{\mathsf{x},1}\mathrm{d}/\mathrm{d}t + \mathrm{d}^2/\mathrm{d}t^2\right) q_{\mathsf{x}} + \mathcal{I}_{yy} q_\theta\,. \quad (4.7)$$

The state space representation in the new variable ζ_{x} is (*cf.* (4.6) and (4.2)):

$$\frac{\mathrm{d}}{\mathrm{d}t}\zeta_{\mathsf{x}} = A_{F_{\mathsf{x}}}\zeta_{\mathsf{x}} + B_{\mathsf{x}}(\bar{u}_{\mathsf{x}} + q_{\mathsf{x},*})\,, \quad \mathsf{x} = C_{\mathsf{x}}\zeta_{\mathsf{x}}\,. \quad (4.8)$$

and its transfer function is:

$$\mathsf{F}_{\zeta_{\mathsf{x}}}(\mathrm{s}) = C_{\mathsf{x}}\big(\mathrm{s}\mathrm{I} - A_{F_{\mathsf{x}}}\big)^{-1} B_{\mathsf{x}} = -\frac{g}{\mathcal{I}_{yy}\pi_{x_{\mathsf{x}}}(\mathrm{s})}. \quad (4.9)$$

Thus, the *exact structural feedback linearization* is: $\bar{u}_{\mathsf{x}} = -q_{\mathsf{x},*}(x(t),\, u(t))$.

C. Robust Asymptotic Feedback Linearization

The observer for rejecting the *nonlinear uncertainty signal* $q_{\mathsf{x},*}$ is (*cf.* (3.11)):

$$\begin{array}{c} \frac{\mathrm{d}}{\mathrm{d}t} w_{\mathsf{x}} = \Big(A_{K_{\mathsf{x}}} + B_{\mathsf{x}} G_{\mathsf{x}}^\ell C_{\mathsf{x}}\Big) w_{\mathsf{x}} - \Big(K_{\mathsf{x}} + B_{\mathsf{x}} G_{\mathsf{x}}^\ell\Big)\mathsf{x}, \\ \bar{u}_{\mathsf{x}} = G_{\mathsf{x}}^\ell\, C_{\mathsf{x}}\, w_{\mathsf{x}} - G_{\mathsf{x}}^\ell\, \mathsf{x}, \end{array} \quad (4.10)$$

where:

$$A_{K_{\mathsf{x}}} = A_{F_{\mathsf{x}}} + K_{\mathsf{x}} C_{\mathsf{x}}\,,\ G_{\mathsf{x}}^\ell = -\left(C_{\mathsf{x}} A_{K_{\mathsf{x}}}^{-1} B_{\mathsf{x}}\right)^\ell = -\frac{\mathcal{I}_{yy}\, a_{\mathsf{x}_o,4}}{g},$$

$$K_{\mathsf{x}} = \begin{bmatrix} a_{\mathsf{x},3} & a_{\mathsf{x},2} & -a_{\mathsf{x},1}\, g & -g \\ a_{\mathsf{x},2} & a_{\mathsf{x},1} & -g & 0 \\ a_{\mathsf{x},1} & 1 & 0 & 0 \\ 1 & 0 & 0 & 0 \end{bmatrix}^{-1} \begin{bmatrix} a_{\mathsf{x},4} - a_{\mathsf{x}_o,4} \\ a_{\mathsf{x},3} - a_{\mathsf{x}_o,3} \\ a_{\mathsf{x},2} - a_{\mathsf{x}_o,2} \\ a_{\mathsf{x},1} - a_{\mathsf{x}_o,1} \end{bmatrix}. \quad (4.11)$$

The characteristic polynomial of the remainder generator (3.12) is:

$$\begin{array}{rcl} \pi_{e_{\mathsf{x}}}(\mathrm{s}) & = & \det(\mathrm{s}\mathrm{I} - A_{K_{\mathsf{x}}}) \\ & = & \mathrm{s}^4 + a_{\mathsf{x}_o,1}\mathrm{s}^3 + a_{\mathsf{x}_o,2}\mathrm{s}^2 + a_{\mathsf{x}_o,3}\mathrm{s} + a_{\mathsf{x}_o,4}\,. \end{array} \quad (4.12)$$

The transfer function of (4.10) is:

$$\mathsf{F}_{w_{\mathsf{x}}}(\mathrm{s}) = \frac{\mathcal{I}_{yy}\, a_{\mathsf{x}_{o,4}}}{g}\, \frac{\pi_{x_{\mathsf{x}}}(\mathrm{s})}{\mathrm{s}\,\bar{\pi}_{w_{\mathsf{x}}}(\mathrm{s})}\,, \tag{4.13}$$

$$\bar{\pi}_{w_{\mathsf{x}}}(\mathrm{s}) = \mathrm{s}^3 + a_{\mathsf{x}_{o,1}}\,\mathrm{s}^2 + a_{\mathsf{x}_{o,2}}\,\mathrm{s} + a_{\mathsf{x}_{o,3}}\,, \tag{4.14}$$

Let us note that (*cf.* (4.14) and (4.12)):

$$\pi_{e_{\mathsf{x}}}(\mathrm{s}) = \mathrm{s}\,\bar{\pi}_{w_{\mathsf{x}}}(\mathrm{s}) + a_{\mathsf{x}_{o,4}}\,. \tag{4.15}$$

So, following a root locus procedure, both polynomials, $\pi_{e_{\mathsf{x}}}(\mathrm{s})$ and $\bar{\pi}_{w_{\mathsf{x}}}(\mathrm{s})$, can be made Hurwitz.

D. Closed Loop System

Defining the error signal, $e_{\mathsf{x}} = w_{\mathsf{x}} - \zeta_{\mathsf{x}}$, we get the closed loop state space representation (*cf.* (4.8) and (4.10)):

$$\frac{\mathrm{d}}{\mathrm{d}t}\begin{bmatrix} e_{\mathsf{x}} \\ \zeta_{\mathsf{x}} \end{bmatrix} = A_{_{CL}}\begin{bmatrix} e_{\mathsf{x}} \\ \zeta_{\mathsf{x}} \end{bmatrix} + B_{_{CL}}\, q_{\mathsf{x},*}\,, \quad \mathsf{x} = C_{_{CL}}\begin{bmatrix} e_{\mathsf{x}} \\ \zeta_{\mathsf{x}} \end{bmatrix}, \tag{4.16}$$

$$A_{_{CL}} = \left[\begin{array}{c|c} A_{K_{\mathsf{x}}} & 0 \\ \hline B_{\mathsf{x}} G_{\mathsf{x}}^{\ell} C_{\mathsf{x}} & A_{F_{\mathsf{x}}} \end{array}\right],\; B_{_{CL}} = \left[\begin{array}{c} -B_{\mathsf{x}} \\ \hline B_{\mathsf{x}} \end{array}\right], \quad C_{_{CL}} = \begin{bmatrix} 0 \mid C_{\mathsf{x}} \end{bmatrix}. \tag{4.17}$$

The transfer functions are (recall (4.12), (4.9) and (4.15)):

$$\mathsf{F}_{e_{\mathsf{x}}}(\mathrm{s}) = G_{\mathsf{x}}^{\ell}\, C_{\mathsf{x}}\,(\mathrm{s}\mathrm{I} - A_{K_{\mathsf{x}}})^{-1}\, B_{\mathsf{x}} = \frac{a_{\mathsf{x}_{o,4}}}{\pi_{e_{\mathsf{x}}}(\mathrm{s})} \tag{4.18}$$

$$\begin{aligned} \mathsf{F}_{_{CL}}(\mathrm{s}) &= C_{_{CL}}\,(\mathrm{s}\mathrm{I} - A_{_{CL}})^{-1}\, B_{_{CL}} \\ &= \begin{bmatrix} 0 \,|\, C_{\mathsf{x}} \end{bmatrix} \cdot \\ &\left[\begin{array}{c|c} (\mathrm{s}\mathrm{I} - A_{K_{\mathsf{x}}})^{-1} & 0 \\ \hline (\mathrm{s}\mathrm{I} - A_{F_{\mathsf{x}}})^{-1} B_{\mathsf{x}} G_{\mathsf{x}}^{\ell} C_{\mathsf{x}} (\mathrm{s}\mathrm{I} - A_{K_{\mathsf{x}}})^{-1} & (\mathrm{s}\mathrm{I} - A_{F_{\mathsf{x}}})^{-1} \end{array}\right] \\ &\cdot \left[\begin{array}{c} -B_{\mathsf{x}} \\ \hline B_{\mathsf{x}} \end{array}\right] \end{aligned}$$

$$\begin{aligned} \mathsf{F}_{_{CL}}(\mathrm{s}) &= \mathsf{F}_{\zeta_{\mathsf{x}}}(\mathrm{s})\Big(1 - \mathsf{F}_{e_{\mathsf{x}}}(\mathrm{s})\Big) = -\frac{g}{\mathcal{I}_{yy}\pi_{x_{\mathsf{x}}}(\mathrm{s})}\left(1 - \frac{a_{\mathsf{x}_{o,4}}}{\pi_{e_{\mathsf{x}}}(\mathrm{s})}\right) \\ &= -\frac{g}{\mathcal{I}_{yy}\pi_{x_{\mathsf{x}}}(\mathrm{s})}\left(\frac{\mathrm{s}\,\bar{\pi}_{w_{\mathsf{x}}}(\mathrm{s})}{\pi_{e_{\mathsf{x}}}(\mathrm{s})}\right), \end{aligned} \tag{4.19}$$

The transfer function (4.19) of the closed loop state space representation, (4.16) and (4.17), has incorporated the high-pass filter:

$$\mathsf{G}_{\text{HPF}_{\mathsf{x}}}(\mathrm{s}) = 1 - \mathsf{F}_{e_{\mathsf{x}}}(\mathrm{s}) = 1 - a_{\mathsf{x}_{o,4}}/\pi_{e_{\mathsf{x}}}(\mathrm{s}) = \mathrm{s}\,\bar{\pi}_{w_{\mathsf{x}}}(\mathrm{s})/\pi_{e_{\mathsf{x}}}(\mathrm{s}). \tag{4.20}$$

Hence, if the *nonlinear uncertainty signal* $q_{\mathsf{x},*}$ has a finite bandwidth, it is then sufficient to synthesize the high-pass filter with a cutoff frequency sufficiently higher than the bandwidth of $q_{\mathsf{x},*}$.

V. NUMERICAL SIMULATIONS

The numerical values of our laboratory prototype are:

$$\begin{gathered} M_q = 1.36\,[\mathrm{kg}],\; g = 9.81\,[\mathrm{m\,s^{-2}}],\; \mathcal{I}_{xx} = 0.0134\,[\mathrm{kg\,m^2}], \\ \mathcal{I}_{yy} = 0.0140\,[\mathrm{kg\,m^2}],\; \mathcal{I}_{zz} = 0.0256\,[\mathrm{kg\,m^2}], \end{gathered} \tag{5.1}$$

and: $L_m = 0.245$ [m], $k_\tau = 4.31 \times 10^{-9}$ [N m/rpm^2], $k_f = 1.98 \times 10^{-7}$ [N/rpm^2] and $\gamma = k_\tau/k_f = 0.0218$ [m].

A. Locally Stabilizing Feedbacks

The state feedbacks were computed by LQR techniques, namely by solving the algebraic Riccati equation,

$$A^T P + PA - PB(\rho\,\mathrm{I})^{-1}B^T P + Q = 0,$$

with the following matrices choices:

$$Q_{\mathsf{x}} = Q_{\mathsf{y}} = 900\begin{bmatrix} 1 & 0 & 0 & 0 \\ 0 & 0 & 0 & 0 \\ 0 & 0 & 1 & 0 \\ 0 & 0 & 0 & 2.25 \end{bmatrix},\; Q_{\mathsf{z}} = \begin{bmatrix} 1 & 0 \\ 0 & 0.23 \end{bmatrix},$$
$$Q_{\psi} = \begin{bmatrix} 1 & 0 \\ 0 & 0.6 \end{bmatrix},\; (\rho_{\mathsf{x}}, \rho_{\mathsf{y}}, \rho_{\mathsf{z}}, \rho_{\psi}) = \big(1, 1, \tfrac{1}{19600}, \tfrac{1}{12100}\big).$$

The optimal state feedbacks are:

$$\begin{aligned} F_{\mathsf{x}} &= \begin{bmatrix} 30 & 32.4264 & -171.9158 & -45.0535 \end{bmatrix}, \\ F_{\mathsf{y}} &= \begin{bmatrix} -30 & -32.4260 & -171.9116 & -45.0512 \end{bmatrix}, \\ F_{\mathsf{z}} &= \begin{bmatrix} -140 & -69.92 \end{bmatrix},\; F_{\psi} = \begin{bmatrix} -110 & -85.2387 \end{bmatrix}. \end{aligned} \tag{5.2}$$

The spectrums of $A_{F_{\mathsf{x}}}$, $A_{F_{\mathsf{y}}}$, $A_{F_{\mathsf{z}}}$ and $A_{F_{\psi}}$ are:

$$\begin{aligned} \Lambda_{\mathsf{x}}(\mathrm{s}) &= \{-3214, -1.911, -0.9536 \pm 1.585\jmath\}, \\ \Lambda_{\mathsf{y}}(\mathrm{s}) &= \{-3358, -1.911, -0.9536 \pm 1.585\jmath\}, \\ \Lambda_{\mathsf{z}}(\mathrm{s}) &= \{-2.087, -49.32\},\; \Lambda_{\psi}(\mathrm{s}) = \{-1.291, -3328\}. \end{aligned} \tag{5.3}$$

The spectrum sets Λ_{x} and Λ_{y} are lower bounded by: $\varrho_\ell = \sqrt{0.9536^2 + 1.585^2} = 1.85$. The characteristic polynomial (4.4) is:

$$\pi_{x_{\mathsf{x}}}(\mathrm{s}) = \mathrm{s}^4 + 3218\,\mathrm{s}^3 + 12279\,\mathrm{s}^2 + 22722\,\mathrm{s} + 21022\,. \tag{5.4}$$

B. Nonlinear Uncertainty Signals *Observation*

Since the quadrotor is planned to move on a (x,y)-plan over a fixed altitude, $\mathsf{z} = \bar{\mathsf{z}}$, we only synthesize *nonlinear uncertainty signals* observers for $q_{\mathsf{x},*}$ and $q_{\mathsf{y},*}$.

1) Observation's dynamics: The dynamics of the remainder generator (3.12) and the *nonlinear uncertainty signal* observer (4.10) are given by the polynomials (4.12) and (4.14), respectively; these two polynomials are related by (4.15). Following a root locus procedure, we get:[4]

$$\begin{aligned} &\bar{\mathrm{s}}\,(\bar{\mathrm{s}} + 4.75)(\bar{\mathrm{s}} + 4)(\bar{\mathrm{s}} + 3.5) + 28.125 = \\ &\qquad (\bar{\mathrm{s}} + 1)^2\,(\bar{\mathrm{s}}^2 + 10.25\,\bar{\mathrm{s}} + 28.125)\,. \end{aligned} \tag{5.5}$$

Scaling the polynomials (5.5) by a factor ϱ_c, 40 times the lower bounded ϱ_ℓ, we get ($\mathrm{s} = \varrho_c\,\bar{\mathrm{s}}$, $\varrho_c = 40\,\varrho_\ell = 74$):

$$\begin{aligned} \mathrm{s}\,\bar{\pi}_{w_{\mathsf{x}}}(\mathrm{s}) &= \mathrm{s}\,(\mathrm{s} + 4.75\,\varrho_c)(\mathrm{s} + 4\,\varrho_c)(\mathrm{s} + 3.5\,\varrho_c) \\ \pi_{e_{\mathsf{x}}}(\mathrm{s}) &= (\mathrm{s} + \varrho_c)^2\,(\mathrm{s}^2 + 10.25\,\varrho_c\,\mathrm{s} + 28.125\,\varrho_c^2)\,. \end{aligned} \tag{5.6}$$

In Fig 1, we show the Bode plot of the high-pass filter $\mathsf{G}_{\text{HPF}_{\mathsf{x}}}(\jmath\,\omega)$, (4.20) and (5.6). The cutoff frequency ω_c of the Bode plot, of the high-pass filter $\mathsf{G}_{\text{HPF}_{\mathsf{x}}}(\jmath\,\omega)$, (4.20) and (5.6),

[4]The natural frequency and the damping ratio of the second order factor are respectively: $\omega_n = 5.3\,\mathrm{rad/s}$ and $\varrho = 0.966$.

is (recall (4.12), (4.20), (5.5) and (5.6)):[5]

$$\begin{aligned}\omega_c &= \sqrt{a_{\mathsf{x}_o,2}/2}\sqrt{1-\sqrt{1-2\,a_{\mathsf{x}_o,4}/a_{\mathsf{x}_o,2}^2}} \\ &= 0.5339\,\varrho_c = 39.5\,\mathrm{rad/s}\,.\end{aligned} \tag{5.7}$$

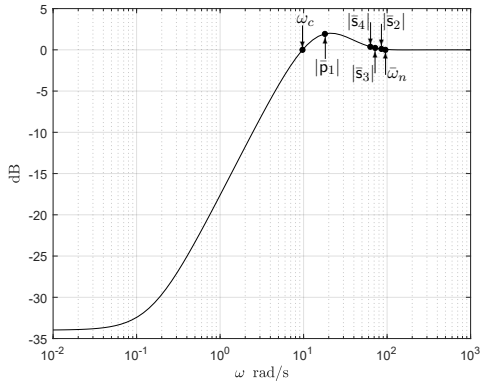

Fig. 1. Bode plot of $\mathsf{G}_{\mathsf{HPF}_\mathsf{x}}(\jmath\,\omega)$, (4.20) and (5.6). $|\bar{\mathsf{p}}_1| = 18$, $|\bar{\mathsf{s}}_2| = 85.5$, $|\bar{\mathsf{s}}_3| = 72$, $|\bar{\mathsf{s}}_4| = 63$, $\bar{\omega}_n = 95.46\,\mathrm{rad/s}$, $\bar{\zeta} = 0.966$ y $\omega_c = 9.7\,\mathrm{rad/s}$.

2) Beard-Jones filter: For simplicity, the Beard-Jones filter (4.10) is synthesized in its *observer canonical form* [5]:

$$\begin{aligned}\tfrac{\mathrm{d}}{\mathrm{d}t}\overline{w}_\mathsf{x} &= \left(\overline{A}_{\overline{K}_\mathsf{x}} + \overline{B}_\mathsf{x} G_\mathsf{x}^\ell \overline{C}_\mathsf{x}\right)\overline{w}_\mathsf{x} - \left(\overline{K}_\mathsf{x} + \overline{B}_\mathsf{x} G_\mathsf{x}^\ell\right)\mathsf{x}\,, \\ \bar{u}_\mathsf{x} &= G_\mathsf{x}^\ell\,\overline{C}_\mathsf{x}\,\overline{w}_\mathsf{x} - G_\mathsf{x}^\ell\,\mathsf{x}\,,\end{aligned} \tag{5.8}$$

where: $\overline{A}_{\overline{K}_\mathsf{x}} = \overline{A}_\mathsf{x} + \overline{K}_\mathsf{x}\overline{C}_\mathsf{x}$, and (recall (5.1), (4.4), (5.4), (4.12) and (5.6)):[6]

$$\overline{A}_\mathsf{x} = \begin{bmatrix} 0 & 0 & 0 & -a_{\mathsf{x},4} \\ 1 & 0 & 0 & -a_{\mathsf{x},3} \\ 0 & 1 & 0 & -a_{\mathsf{x},2} \\ 0 & 0 & 1 & -a_{\mathsf{x},1} \end{bmatrix},\ \left(\overline{B}_\mathsf{x}, \overline{C}_\mathsf{x}, \overline{K}_\mathsf{x}\right) =$$

$$\left(\begin{bmatrix} -g/Iyy \\ 0 \\ 0 \\ 0 \end{bmatrix}, \begin{bmatrix} 0 \\ 0 \\ 0 \\ 1 \end{bmatrix}^T, \begin{bmatrix} a_{\mathsf{x},4} - a_{\mathsf{x}_o,4} \\ a_{\mathsf{x},3} - a_{\mathsf{x}_o,3} \\ a_{\mathsf{x},2} - a_{\mathsf{x}_o,2} \\ a_{\mathsf{x},1} - a_{\mathsf{x}_o,1} \end{bmatrix}\right),$$

$$G_\mathsf{x}^\ell = -\left(\overline{C}_\mathsf{x}\,\overline{A}_{\overline{K}_\mathsf{x}}^{-1}\,\overline{B}_\mathsf{x}\right)^\ell = -(a_{\mathsf{x}_o,4}\mathcal{I}_{yy})/g,$$

$$\overline{K}_\mathsf{x} = \begin{bmatrix} -843351429 & -26924674 & -259467 & 2311.6 \end{bmatrix}^T. \tag{5.9}$$

C. Simulation Results

In Fig. 2, we show some simulation results obtained in a MATLAB® platform. We have considered that the earth axes

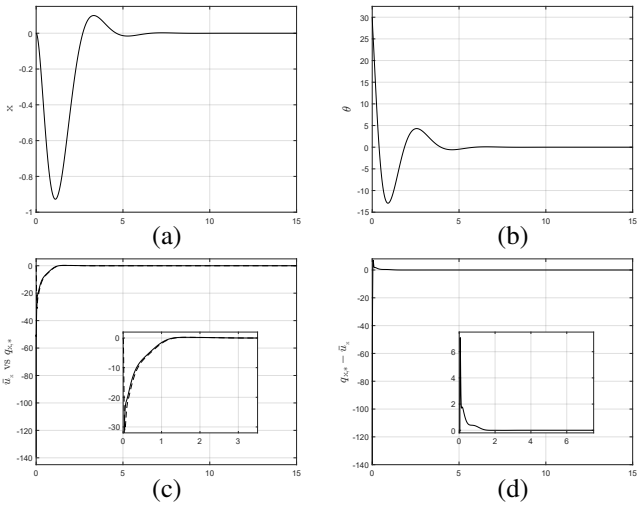

Fig. 2. (a) Horizontal position, x [m]. (b) Pitch position, θ [°]. (c) Estimated *nonlinear uncertainty signal* (*cf.* (5.8) and (5.9)), $\bar{u}_\mathsf{x}$ *vs* computed *nonlinear uncertainty signal* (*cf.* (4.7), (2.6)–(2.8)), $q_{\mathsf{x},*}$. (d) Estimation error, $q_{\mathsf{x},*} - \bar{u}_\mathsf{x}$.

$(o\mathsf{xyz})$ is located at height $\bar{\mathsf{z}} = 2\,[\mathrm{m}]$, above the ground level, and with the initial conditions: $\mathsf{x}(0) = \mathsf{y}(0) = \mathsf{z}(0) = 0$ [m], $\mathrm{d}\mathsf{x}(0)/\mathrm{d}t = \mathrm{d}\mathsf{y}(0)/\mathrm{d}t = \mathrm{d}\mathsf{z}(0)/\mathrm{d}t = 0\,[\mathrm{m\,s^{-1}}]$, $\phi(0) = \theta(0) = \psi(0) = \alpha_0$, $\alpha_0 = \pi/6$ [rad], $\mathrm{d}\phi(0)/\mathrm{d}t = \mathrm{d}\theta(0)/\mathrm{d}t = \mathrm{d}\psi(0)/\mathrm{d}t = 0\,[\mathrm{rad\,s^{-1}}]$.

The initial conditions of the Beard-Jones filter (5.8) and (5.9) were set up as (*cf.* [2]):

$$\begin{aligned}\overline{w}_\mathsf{x}(0) &= -\begin{bmatrix} a_{\mathsf{x},1}g & g & 0 & 0 \end{bmatrix}^T \tan\alpha_0\,(\cos\alpha_0 + \tan\alpha_0)\,, \\ \overline{w}_\mathsf{y}(0) &= \begin{bmatrix} a_{\mathsf{y},1}g & g & 0 & 0 \end{bmatrix}^T \tan\alpha_0\,(1 - \sin\alpha_0)\,, \\ \overline{w}_\psi(0) &= \begin{bmatrix} \alpha_0 a_{\psi,1} & \alpha_0 \end{bmatrix}^T.\end{aligned} \tag{5.10}$$

From Fig. 2, we can verify that the *nonlinear uncertainty signal* estimation $\bar{u}_{,\mathsf{x}}$, obtained *via* the Beard-Jones filter (5.8) and (5.9), closely follows the *nonlinear uncertainty signal* $q_{\mathsf{x},*}$, computed *via* (4.7), (2.6)–(2.8).

VI. EXPERIMENTAL RESULTS

In Fig. 3, we show some experimental results obtained in open field; we compare the horizontal position trajectories x: *(i)* when both control laws are applied, the locally stabilizing feedback $F_\mathsf{x}x_\mathsf{x}$ (4.1) and (5.2) plus the estimation of the *nonlinear uncertainty signal* $\bar{u}_\mathsf{x}$ (5.8) and (5.9) (solid line), and *(ii)* when only the locally stabilizing feedback $F_\mathsf{x}x_\mathsf{x}$ (4.1) and (5.2) is applied. From this figure, we can point out the correct rejection of the *nonlinear uncertainty signal* $q_{\mathsf{x},*}$, *via* the Beard-Jones filter (5.8) and (5.9).

VII. CONCLUSION

In [1], we have shown that for a system modeled by the state space representation (3.1), where q is an *uncertainty signal*, and the map S is contained in the image of B, namely there exists a Q such that: $S = BQ$, then the *uncertainty signal* q can be rejected by means of the Beard-Jones filter (3.11). Such proposition was tested *via* the altitude control

[5] Doing: $|\mathsf{G}_{\mathsf{HPF}_\mathsf{x}}(\jmath\,\omega)| = 1$, one gets: $2a_{\mathsf{x}_o,4}\omega^4 - 2a_{\mathsf{x}_o,2}a_{\mathsf{x}_o,4}\omega^2 + a_{\mathsf{x}_o,4}^2 = 0$.

[6] $\overline{w}_\mathsf{x} = T_{o\mathsf{x}}^{-1}w_\mathsf{x}$, $T_{o\mathsf{x}} = \begin{bmatrix} a_{\mathsf{x},3} & a_{\mathsf{x},2} & -a_{\mathsf{x},1}\,g & -g \\ a_{\mathsf{x},2} & a_{\mathsf{x},1} & -g & 0 \\ a_{\mathsf{x},1} & 1 & 0 & 0 \\ 1 & 0 & 0 & 0 \end{bmatrix}^{-1}$, $\left(\overline{A}_\mathsf{x}, \overline{B}_\mathsf{x}, \overline{C}_\mathsf{x}, \overline{K}_\mathsf{x}\right) = \left(T_{o\mathsf{x}}^{-1}A_{F_\mathsf{x}}T_{o\mathsf{x}},\, T_{o\mathsf{x}}^{-1}B_\mathsf{x},\, C_\mathsf{x}T_{o\mathsf{x}},\, T_{o\mathsf{x}}^{-1}K_\mathsf{x}\right)$, $G_\mathsf{x}^\ell = -\left(C_\mathsf{x}\left(A_{F_\mathsf{x}} + K_\mathsf{x}C_\mathsf{x}\right)^{-1}B_\mathsf{x}\right)^\ell = -\left(\overline{C}_\mathsf{x}\,\overline{A}_{\overline{K}_\mathsf{x}}^{-1}\,\overline{B}_\mathsf{x}\right)^\ell$.

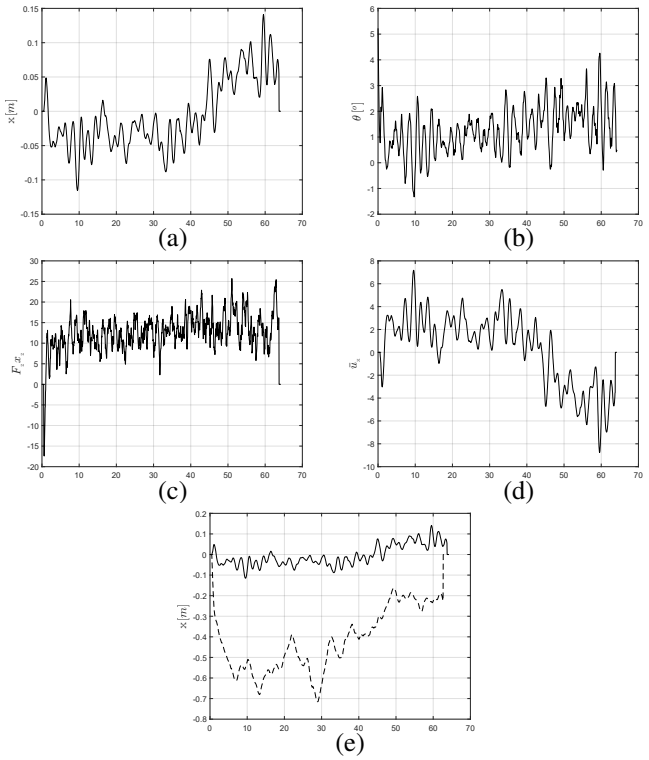

Fig. 3. (a) Horizontal position, x [m]. (b) Pitch position, θ [°]. (c) Locally stabilizing feedback $F_{\mathsf{z}}x_{\mathsf{z}}$ [N m]. (d) Estimated *nonlinear uncertainty signal* (*cf.* (5.8)), $\bar{u}_{\mathsf{x}}$. (e) Comparison of the horizontal positions, x [m], obtained with the application of both, the locally stabilizing feedback $F_{\mathsf{x}}x_{\mathsf{x}}$ (4.1) and (5.2) plus the estimation of the *nonlinear uncertainty signal* $\bar{u}_{\mathsf{x}}$ (5.8) and (5.9) (solid line), against only the application of the locally stabilizing feedback $F_{\mathsf{x}}x_{\mathsf{x}}$ (4.1) and (5.2) (dashed line).

of a planar vertical takeoff and landing (PVTOL) aircraft in a laboratory setting.

In [2], we have shown that the linear control scheme, based on failure detection techniques, introduced in [1] is in fact a structural feedback linearization technique, where the nonlinearities, affecting the systems dynamics, are treated as failure signals. Based on the Brunovsky canonical form [4], we have proposed the change of variable (3.6), for changing from the state space representation in its Brunovsky canonical form to a nice state space representation, where the *uncertainty signal* q_* is inside of the image of the input map, and thus, with a Beard-Jones filter type, q_* is rejected. This control scheme was illustrated with a MATLAB® numerical simulation of a quadrotor in hover flying.

In [3], the two previous results were formalized to the more general nonlinear state space representation (3.1), and we generalized the change of variable (3.6), based on the algebraic equation (3.2), issued from the assumption that the pair (A, B) is controllable. Under such a change of variable, we have obtained once again the state representation (3.7), where the *nonlinear uncertainty signal* (3.8) is contained in the image of B. We have also generalized the previous Beard-Jones filters to the control scheme (3.11).

In this paper, we have shown in detail the synthesis procedure of the control scheme recently proposed in [3]. This control scheme has the advantage of combining the classical linear control techniques with the sophisticated robust control techniques. This control scheme is specially *ad hoc* for unmanned aircraft vehicles, where it is important not only to have the capability of rejecting the actual nonlinearities and the unexpected changes of structure, but also to obtain simplicity and effectiveness of the control scheme.

We have tested the effectiveness and simplicity of our proposition with the quadrotor laboratory prototype, in hover flying, having the numerical values (5.1). In order to tune our control scheme, we have first done some simulation proofs, shown in Section V, and then we have tested our proposition in open field, as shown in Section VI. Because of lack of place, comparison with alternative approaches will be done in an extended version of the present contribution.

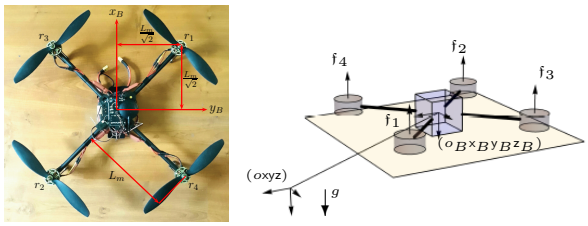

Fig. 4. (a) Quadrotor. (b) Schematic diagram.

REFERENCES

[1] Bonilla, M., Blas, L.A., Salazar, S., Martínez, J.C. and Malabre, M. (2016). A Robust Linear Control Methodology based on Fictitious Failure Rejection. *European Control Conference*, pp. 2596–2601. June 29 - July 1, 2016. Aalborg, Denmark.

[2] Blas, L.A., Bonilla, M., Malabre, M., Azhmyakov, V. and Salazar, S. (2017). *IFAC-World Congress*, pp. 2596–2601. July 9 - 14, 2017. Toulouse, France.

[3] Bonilla, M., Blas, L.A., Azhmyakov, V., Malabre, M. and Salazar, S. (2018). Robust Structural Feedback Linearization Based on the Non-linearities Rejection. *Submitted*, 24 pp.

[4] Brunovsky, P. (1970). A classification of linear controllable systems. *Kybernetika* **6(3)**, 173–188.

[5] Kailath, Th. (1980). **Linear systems**, *Prentice-Hall, New Jersey*.

[6] Lee, D., Kim, H.J., Sastry, Sh. Feedback linearization *vs.* adaptive sliding mode control for a quadrotor helicopter. *International Journal of Control, Automation and Systems* **7(3)**, pp. 419-428, 2009.

[7] Liu, H., Bai, Y., Lu, G., Shi, Z., Zhong, Y. Robust Tracking Control of a Quadrotor Helicopter. *Journal of Intelligent & Robotic Systems* **75**, pp. 595-608, 2014.

[8] Massoumnia, M.A. A geometric approach to the synthesis of failure detection filters, *IEEE Transactions on Automatic Control*, **31(9)**, pp. 839–846, 1986.

[9] Powers, C., Mellinger, D., and Kumar, V. (2014). Quadrotor Kinematics and Dynamics. In Chapter 16 of **Handbook of unmanned aerial vehicles**, editors Valavanis, K. P., & Vachtsevanos, G. J. *New York : Springer Publishing Company, Incorporated*.

[10] Willems, J.C. Input-output and state-space representations of finite-dimensional linear time-invariant systems, *Linear Algebra and its Applications*, **50**, 581–608, 1983.

[11] Willems, J.C. and Polderman, J.W. **Introduction to Mathematical Systems Theory: A Behavioral Approach**, *New York: Springer-Verlag*, 1998.

[12] Wonham, W.M. **Linear Multivariable Control: A Geometric Approach**, *New York: Springer-Verlag, 3rd ed*, 1985.

[13] Zhou, Q.L., Zhang, Y., Rabbath, C.A., and Theilliol, D. Design of Feedback Linearization Control and Reconfigurable Control Allocation with Application to a Quadrotor UAV. *Conference on Control and Fault Tolerant Systems*, pp. 371–376. October 6 - 8, 2010. Nice, France.